

Asymmetry-induced radiative heat transfer in Floquet systems

Hui Pan,^{1,*} Yuhua Ren,¹ Gaomin Tang,^{2,†} and Jian-Sheng Wang^{1,‡}

¹Department of Physics, National University of Singapore, Singapore 117551, Republic of Singapore

²Graduate School of China Academy of Engineering Physics, Beijing 100193, China

(Dated: October 15, 2024)

Traditional fluctuational electrodynamics describing thermal radiation from bodies at local equilibrium may break down in Floquet-driven systems. We develop a general microscopic theory to account for the out-of-equilibrium states of photons induced by electronic fluctuations in periodically driven systems and the associated radiative heat transfer between objects. The nonequilibrium occupation of radiative photons in Floquet states follows an exponential-staircase distribution, with the nonequilibrium thermal distribution sensitive to the electronic properties of the material. We further show significant heat transfer between two parallel metal plates with different microscopic properties, despite identical driving protocols and bath temperatures. This work opens up new opportunities for the directional manipulation of radiative heat transfer in Floquet systems.

Introduction.— The theory of heat transfer due to thermal radiation has been well-established since the time of Rylov and Lifshitz based on fluctuational electrodynamics [1, 2] and, as a cornerstone, by the fluctuation-dissipation theorem [3]. The most significant achievement is the discovery of enhanced near-field radiative heat transfer, which is orders of magnitude larger than that of blackbody radiation [4–10]. The theory of fluctuational electrodynamics assumes local thermal equilibrium for each object. However, recent developments in periodically driven systems go beyond local thermal equilibrium, as such systems fail to obey the fluctuation-dissipation theorem, and a new formulation is an active research topic [11–13]. What the out-of-equilibrium states are is a subtle question, as W. Kohn pointed out, depending on how an isolated system is coupled to the environment [14].

Floquet driving opens up tremendous possibilities for engineering novel material properties, including driving-induced topological order and phase transitions [15–20]. It has been extensively explored in optical systems [21–24], such as photonic time crystals [25–28] and nonreciprocal transport [29–34]. Moreover, employing such systems as basic heat transfer units has attracted significant attention [12, 35–39], such as radiative heat shuttling [40], active radiative cooling [13, 41–43], and nonreciprocal heat transfer [44–46]. However, the nonequilibrium occupation characteristics of radiative photons in Floquet systems, along with their microscopic origins, remain largely unexplored, primarily due to the breakdown of the fluctuation-dissipation theorem. To understand thermal distribution in Floquet systems and study the radiative heat transfer among the objects or into the vacuum necessitates a robust analytical framework, which we identify as the nonequilibrium Green’s function method [13, 47–53]. This formulation naturally answers the questions of out-of-equilibrium distribution.

In this Letter, by combining the nonequilibrium Green’s function formalism with the Floquet theory, we study radiative heat transfer between two parallel metal plates with periodically modulated electron potentials [see Fig. 1]. We find that the occupation of radiative photons in Floquet states exhibits an exponential-staircase distribution. The nonequilibrium thermal distribution is sensitive to the electronic prop-

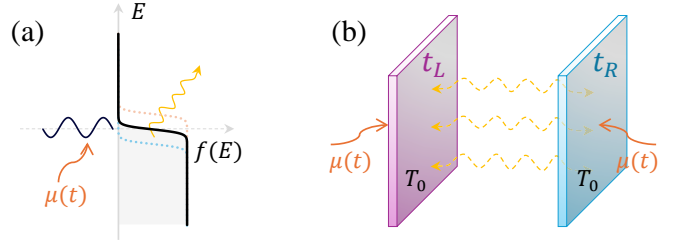


FIG. 1. (a) Schematic of the driving protocol coupling to a time-varying potential $\mu(t) = 2\mu_d \cos(\Omega t)$ with driving frequency Ω and amplitude $2\mu_d$. (b) Illustration of near-field heat radiation between two parallel metal plates with hopping parameters t_L and t_R . Each plate is in contact with an equilibrium bath at temperature T_0 and periodically driven by an identical potential $\mu(t)$. The interplay of differences in material properties and external drivings lead to an imbalance in photon occupation between the plates and, thereby, a finite heat flux.

erties. We further demonstrate that even with identical driving protocols and temperatures, differences in material properties lead to finite heat transfer between the plates due to non-identical nonequilibrium distributions. Such transfer is impossible for systems at local thermal equilibrium, where heat transfer is prohibited under identical temperatures as the second law of thermodynamics dictates.

Formalism.— We briefly describe the theory with details provided in the Supplemental Material [54]. We consider radiative heat transfer between two two-dimensional metal plates in a parallel configuration [see Fig. 1(b)], although the theory applies to arbitrary geometries. In such metal systems, it is the electronic fluctuations that primarily give rise to the exchange of radiative photons between subsystems. The retarded Green’s function of the electrons under a time-varying Hamiltonian satisfies [55]

$$[i\hbar\partial_t - H(t) - \Sigma^r]G^r(t, t') = I\delta(t - t'). \quad (1)$$

In the tight-binding representation, the retarded Green’s function is defined as $G_{jk}^r(t, t') = \theta(t - t')\langle c_j(t)c_k^\dagger(t') + c_k^\dagger(t')c_j(t) \rangle / (i\hbar)$, where $\theta(t)$ is the Heaviside step function, c_j (c_k^\dagger) is the annihilation (creation) operator at electron site

$j(k)$, and $\sum_{jk} c_j^\dagger H_{jk}(t) c_k$ is the many-body electron Hamiltonian. The matrices H and G are indexed by the electron sites. The identity matrix is denoted by I , and $\delta(t)$ is the Dirac delta function. The last term on the left-hand side of the equation is a convolution in the time domain with $\int \Sigma^r(t, t'') G^r(t'', t') dt''$, where the retarded self-energy Σ^r arises from the coupling to the bath. This term is crucial for the thermal distribution in a nonequilibrium setting, as it dictates how the system is coupled to the environment and exchanges energy and electrons.

The lesser component of the electron Green's function $G_{jk}^<(t, t') = (i/\hbar) \langle c_k^\dagger(t') c_j(t) \rangle$ describes the electron distribution. According to the usual Keldysh theory, it is given by the equation $G^< = G^r \Sigma^< G^a$, where $\Sigma^<$ is the lesser self-energy from the bath, and $G^a = (G^r)^\dagger$. The triple product denotes matrix multiplication in the site space and convolution in the time domain. We assume each bath is in thermal equilibrium and has the usual fluctuation-dissipation theorem; in the energy domain, $\Sigma^<(E) = -f(E) [\Sigma^r(E) - \Sigma^a(E)]$ where $f(E) = 1 / \{\exp[(E - \mu_s)/(k_B T_0)] + 1\}$ is the Fermi function at temperature T_0 and chemical potential μ_s . We choose $\Sigma^r = -i\eta I$ with η/\hbar the inverse of electron relaxation time, which implies each site or mode is coupled identically to the bath. It is certainly feasible to model the bath more explicitly, for example, by putting the system on a weakly coupled substrate.

Before discussing the photon Green's function, we first focus on general properties of the periodically driven system [11, 15]. As noted above, the Green's functions depend on two time variables. For steady-state systems with time-translation invariance, the Green's functions depend solely on the time difference, making it convenient to work in the frequency domain. However, this convenience is lost for periodically driven systems. Nonetheless, a residue symmetry persists for an arbitrary function \mathcal{F} with two time variables when we are in a Floquet steady state, denoted as $\mathcal{F}(t + 2\pi/\Omega, t' + 2\pi/\Omega) = \mathcal{F}(t, t')$ where Ω is the driving frequency. This discrete time periodicity can be represented by a double Fourier series as

$$\mathcal{F}(t, t') = \int_{-\Omega/2}^{+\Omega/2} \frac{d\omega}{2\pi} \sum_{mn} \mathcal{F}_{mn}(\omega) e^{-i\omega_m t + i\omega_n t'}, \quad (2)$$

with $\omega_m = \omega + m\Omega$. We note that the Floquet matrix \mathcal{F} satisfies $\mathcal{F}_{mn}(\omega + k\Omega) = \mathcal{F}_{m+k, n+k}(\omega)$.

To describe energy transport mediated by the electromagnetic field, we introduce the photon Green's function defined by vector potential \mathbf{A} [52, 56],

$$D_{\mu\nu}^r(\mathbf{r}, t; \mathbf{r}', t') = \frac{1}{i\hbar} \theta(t - t') \langle [A_\mu(\mathbf{r}, t), A_\nu(\mathbf{r}', t')] \rangle, \quad (3)$$

with $\mu, \nu = x, y, z$ the directions in Cartesian coordinate system. The operators are in the Heisenberg picture, and the square bracket denotes the commutator. In this work, the particular temporal gauge [56, 57] has been chosen. The retarded Green's function satisfies a Dyson equation, expressed

as $D^r = v + v\Pi^r D^r$. Here, v is the free photon Green's function, relating electric current density to the vector potential via $\mathbf{A} = -v\mathbf{j}$, and the retarded photon self-energy Π^r can be interpreted as the linear response of the induced current in matter, $\mathbf{j}^{\text{ind}} = -\Pi^r \mathbf{A}$.

The lesser photon Green's function $D_{\mu\nu}^<(\mathbf{r}, t; \mathbf{r}', t') = \langle A_\nu(\mathbf{r}', t') A_\mu(\mathbf{r}, t) \rangle / (i\hbar)$ describes the photon distribution, given by the Keldysh equation [52],

$$D^< = D^r (\Pi^< + \Pi_\infty^<) D^a. \quad (4)$$

There is a subtlety here as we have two self-energies: the first arises from the actual objects, while the second represents energy dissipation into the vacuum and is given by $\Pi_\infty^r = [-v^{-1} + (v^{-1})^\dagger]/2$. The photon self-energy from actual objects is derived through a diagrammatic expansion with the interaction from the Peierls substitution Hamiltonian, $\sum_{jk} c_j^\dagger H_{jk} c_k \exp[e_0/(i\hbar) \int_{\mathbf{r}_k}^{\mathbf{r}_j} \mathbf{A} \cdot d\mathbf{r}]$ with e_0 the elementary charge, taking the contributions linear in \mathbf{A} with the random phase approximation and quadratic in \mathbf{A} for the diamagnetic term. The final expressions for Π can be expressed as convolutions of two electron Green's functions in the Floquet space, such as $\Pi^< \propto G^< G^>$. Details are provided in the Supplemental Material [54].

The net energy emitted out of object α can be calculated either by integrating the Poynting vector over a surface enclosing the object or by performing a volume integral through the Joule heating formula, $-\mathbf{E} \cdot \mathbf{j}$. We find the latter approach convenient for our purpose. The current density of the object can be expressed in terms of the vector potential as $\mathbf{j} = -\mathbf{A} v^{-1}$ where $v^{-1} = -\epsilon_0 (\partial^2/\partial t^2 + c^2 \nabla \times \nabla \times)$ is a differential operator. Here, c is the speed of light and ϵ_0 the vacuum permittivity. The energy current can be expressed in terms of the photon Green's function as [52, 54]

$$\begin{aligned} I_\alpha(t) &= - \int_\alpha d\mathbf{r} \langle \mathbf{E} \cdot \mathbf{j} \rangle \\ &= - \int_\alpha d\mathbf{r} \frac{\partial}{\partial t} \sum_{\mu, \nu} \langle A_\mu(\mathbf{r}, t) A_\nu(\mathbf{r}, t') \rangle v_{\nu\mu}^{-1}(\mathbf{r}, t') \Big|_{t'=t} \\ &= \int_\alpha d\mathbf{r} \frac{\hbar}{2i} \frac{\partial}{\partial t} [D^K(\mathbf{r}t, \mathbf{r}t') v^{-1}] \Big|_{t'=t}. \end{aligned} \quad (5)$$

The Keldysh Green's function is $D^K = D^< + D^>$ with $D^>$ the greater photon Green's function. Such a symmetric function ensures a real energy current. Using the Dyson equation in the form $D^a v^{-1} = I + D^a \Pi^a$ and the Keldysh equation $D^K = D^r \Pi^K D^a$, we find $D^K v^{-1} = D^r \Pi^K + D^K \Pi^a$. Inserting this into Eq. (5), we obtain the Meir-Wingreen formula for the energy current out of object α . Since the space integral is restricted to object α , we replace the total self-energy Π by the self-energy of object α which is Π_α .

For a periodically driven system, using Eq. (2), we can express the average energy current by the Floquet matrices with [54]

$$\bar{I}_\alpha = - \int_{-\Omega/2}^{+\Omega/2} \frac{d\omega}{4\pi} \text{Tr} [E (D^r \Pi_\alpha^K + D^K \Pi_\alpha^a)]. \quad (6)$$

Here, \mathbf{D} and $\mathbf{\Pi}$ are Floquet matrices of the photon Green's function and self-energy, respectively. The entries of diagonal matrix \mathbf{E} are $E_{mn} = \hbar\omega_m\delta_{mn}$. The trace is over direction μ , electron site, and Floquet index m . Using the relation $\mathcal{F}_{mn}(\omega + k\Omega) = \mathcal{F}_{m+k, n+k}(\omega)$, Eq. (6) can be rewritten as

$$\bar{I}_\alpha = - \int_{-\infty}^{+\infty} \frac{d\omega}{4\pi} \text{Tr} [\hbar\omega (\mathbf{D}' \mathbf{\Pi}_\alpha^K + \mathbf{D}^K \mathbf{\Pi}_\alpha^a)_{00}], \quad (7)$$

where the integral of ω is expanded from $(-\Omega/2, +\Omega/2)$ to the entire frequency range, with the trace taken over the “00” block of the Floquet matrix. This transform facilitates us in accessing the spectrum of heat current.

Photon distribution in Floquet states.— We now apply our formalism to investigate the nonequilibrium distribution of radiative photons in Floquet states. As shown in Fig. 2(a), we consider a metal plate with hopping parameter t_0 and temperature T_0 . The chemical potential is periodically modulated with $\mu(t) = 2\mu_d \cos(\Omega t)$. In this work, the static chemical potential is set to be $\mu_s = 0$. Unless specified otherwise, we use $t_0 = 1.0$ eV, $\eta = 0.1$ eV, $\hbar\Omega = 1.0$ eV, and $\mu_d = 0.1$ eV in numerical calculations. Excluding energy dissipation into the vacuum, the effective photon occupation \bar{N} is given by $\bar{N}(\mathbf{q}, \omega) = \text{Tr} \{ \text{Im} [\mathbf{\Pi}_{00}^<(\mathbf{q}, \omega)] \} / 2 \text{Tr} \{ \text{Im} [\mathbf{\Pi}_{00}^r(\mathbf{q}, \omega)] \}$, with $\mathbf{q} = (q_x, q_y)$ the photon wavevector. The frequency-dependent distribution, denoted by $\bar{N}(\omega)$, can be obtained by summing over \mathbf{q} in both the numerator and denominator.

As depicted in Fig. 2(b), the effective photon distribution is simply the Bose-Einstein distribution at $T = 300$ K, $N_B(\omega, T) = 1 / [\exp(\hbar\omega/k_B T) - 1]$ for the undriven case. In the driven case, however, the photon occupation exhibits an exponential-staircase distribution, with step edges at integer multiples of Ω . Moreover, the photons reach an effective temperature of about 2000 K, indicating a pumping effect of the Floquet driving. It is noteworthy that the exponential-staircase distribution is a key characteristic of radiative photons in Floquet states. Furthermore, the effective photon distribution can be expressed as a weighted sum of the Floquet-Fermi-Dirac distribution \bar{f} (see Supplemental Material [54] for details) and given by

$$\bar{N}(\mathbf{q}, \omega) = \frac{\sum_{\mathbf{k}} W_{\mathbf{k}, \mathbf{q}}(\omega) \bar{f}(\varepsilon_{\mathbf{k}}) [1 - \bar{f}(\varepsilon_{\mathbf{k}} - \hbar\omega)]}{\sum_{\mathbf{k}} W_{\mathbf{k}, \mathbf{q}}(\omega) [\bar{f}(\varepsilon_{\mathbf{k}} - \hbar\omega) - \bar{f}(\varepsilon_{\mathbf{k}})]}. \quad (8)$$

Here, $W_{\mathbf{k}, \mathbf{q}}(\omega) = |V_{\mathbf{k}, \mathbf{q}}|^2 \delta(\varepsilon_{\mathbf{k}} - \varepsilon_{\mathbf{k}-\mathbf{q}} - \hbar\omega)$ is the weight function constraining the scattering channel with amplitude $V_{\mathbf{k}, \mathbf{q}} = (\mathbf{v}_{\mathbf{k}} + \mathbf{v}_{\mathbf{k}-\mathbf{q}}) / 2$, where $\mathbf{v}_{\mathbf{k}}$ is the electron group velocity. In Fig. 2(b), the effective distribution from Eq. (8) closely matches that calculated from self-energies Π .

To connect the effective photon distribution to radiative heat transfer, we define the effective photon temperature \bar{T} by the local equilibrium assumption in the frequency domain, $N_B(\omega, \bar{T}) = \bar{N}(\mathbf{q}, \omega)$. Here, we adopt an alternative definition of \bar{N} , specifically $\bar{N}(\mathbf{q}, \omega) = \text{Tr} \{ \text{Im} [\mathbf{D}_{00}^<(\mathbf{q}, \omega)] \} / 2 \text{Tr} \{ \text{Im} [\mathbf{D}_{00}^r(\mathbf{q}, \omega)] \}$, to simultaneously capture both propagating and evanescent modes. In

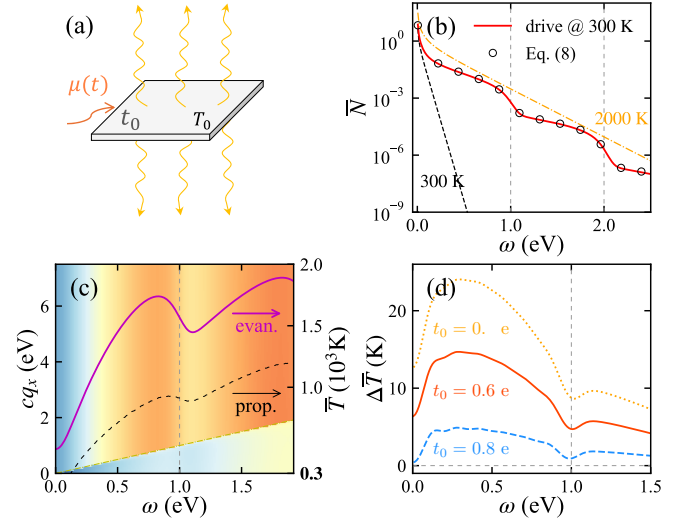


FIG. 2. (a) Illustration of heat radiation from a metal plate with hopping parameter t_0 , bath temperature T_0 , and the chemical potential periodically modulated as $\mu(t)$. (b) Effective photon distribution \bar{N} for the metal plate in driven (solid line and circles) and undriven (dashed line for 300 K and dash-dotted line for 2000 K) cases. (c) Effective photon temperature \bar{T} in the (q_x, ω) space (background map). The corresponding \bar{T} spectrum is shown for evanescent (labeled “evan.”) and propagating (labeled “prop.”) modes. (d) Difference in effective temperature spectra between plates with different t_0 : $\Delta\bar{T}(\omega) = \bar{T}(\omega; 1 \text{ eV}) - \bar{T}(\omega; t_0)$.

the one-plate setup, this definition yields the same \bar{N} for the evanescent modes as obtained from the self-energies Π . As shown in Fig. 2(c), the light line separates the $\bar{T}(\mathbf{q}, \omega)$ into the propagating ($c|\mathbf{q}| < \omega$) and evanescent ($c|\mathbf{q}| > \omega$) regions. The propagating modes exhibit lower effective temperatures than the evanescent modes due to heat dissipation into the vacuum. Since the heat transfer is dominated by photons with energy below 1.0 eV under our chosen parameters, we restrict our analysis to the frequency range $\omega \in [0, \Omega]$.

A notable feature in this region is the increasing effective temperature \bar{T} with photon frequency ω , suggesting that a metal plate with a higher plasmon frequency possesses a greater \bar{T} , regardless of the identical bath temperatures and driving protocols. To demonstrate this, we plot the effective-temperature differences $\Delta\bar{T}$ for metal plates with various t_0 in Fig. 2(d), using the result of \bar{T} for $t_0 = 1.0$ eV as the baseline. The periodic modulation results in a finite $\Delta\bar{T}$ (up to 10 K for $t_0 = 0.6$ eV) between different metal plates, in spite of the effective electron distribution \bar{f} remaining constant with t_0 . This phenomenon results in a remarkable consequence: a global periodic driving could induce a finite radiative heat transfer between two asymmetric metal plates despite identical bath temperatures.

Asymmetry-induced radiative heat transfer.— We now examine the above inference by studying radiative heat transfer between two parallel metal plates, as illustrated in Fig. 1(b). The plates have the same bath temperature $T_0 = 300$ K but different hopping parameters (t_L and t_R). We set $t_L = 1.0$

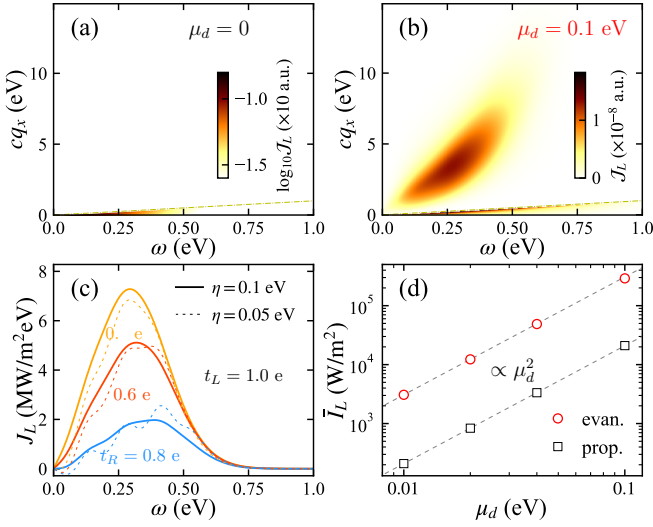


FIG. 3. Radiative heat flux maps of the left plate \mathcal{J}_L in the two-plate system for (a) undriven and (b) driven cases with separation distance $d = 53$ nm. (c) Heat flux spectrum J_L contributed by evanescent modes at various t_R and η in the driven case. (d) Heat fluxes \bar{I}_L contributed by evanescent (red circles) and propagating (black squares) modes, both proportional to μ_d^2 (dashed lines) for $\mu_d \ll \hbar\Omega$.

eV and $t_R = 0.6$ eV unless stated otherwise. We focus solely on the heat flux out of the left plate, as the heat-flux maps satisfy the relation $\mathcal{J}_R(\mathbf{q}, \omega) = -\mathcal{J}_L(\mathbf{q}, \omega)$ for the evanescent modes, with contributions from the propagating modes being negligible in the near-field regime. Figures 3(a) and 3(b) show the heat-flux maps, $\mathcal{J}_L(q_x, \omega) = q_x \hbar \omega \text{Tr}[(\mathbf{D}^r \mathbf{\Pi}_L^K + \mathbf{D}^K \mathbf{\Pi}_L^a)_{00}]$, in the undriven and driven cases, respectively. In contrast to the undriven case, the periodic driving results in a finite heat flux contributed by the evanescent modes, consistent with our analysis of the effective photon distribution. It is noteworthy that the driving does not introduce net energy into the steady-state system [13]; it facilitates heat transfer from one side to the other.

To examine the dependence of heat transfer on the microscopic parameters, we now study the heat-flux spectra for various t_R and damping parameters η . The heat-flux spectrum contributed by the evanescent modes is given by $J_L(\omega) = \int_0^{\pi/a} dq_x \theta(cq_x - \omega) \mathcal{J}_L(q_x, \omega) / (2\pi)$, with a the lattice constant. Figure 3(c) demonstrates that increasing the difference in hopping parameters leads to a larger $\Delta\bar{T}$ [see Fig. 2(d)] and, thereby, a higher heat flux density. However, further increasing this difference results in a decreased heat flux density due to the mismatch of the plasmon frequencies (see Supplemental Material [54] for details). The magnitude of heat flux density depends on the interplay between $\Delta\bar{T}$ and the effective transmission. Moreover, the heat flux density is not sensitive to the damping parameter η as seen from Fig. 3(c). We also discuss the effect of the driving amplitude $2\mu_d$ which determines the deviation of a driven system from its equilibrium state. As depicted in Fig. 3(d), both contributions from the evanescent and the propagating modes to the heat fluxes are proportional

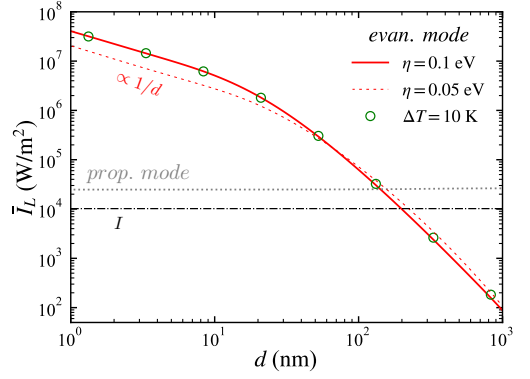


FIG. 4. Distance dependence of heat flux out of the left plate. For comparison, heat flux calculated using the Landauer formula with $T_{L(R)} = 1650 \text{ K} \pm 5 \text{ K}$ is shown as circles. The corresponding blackbody radiation heat flux I_{bb} is also shown according to the Stefan-Boltzmann law.

to μ_d^2 for $\mu_d \ll \hbar\Omega$. Applying the analytical formula Eq. (8) for a two-level model, we demonstrate that this dependency is due to the fact that $\bar{N} \propto \mu_d^2$ [54].

Finally, we show the distance dependence of the heat transfer. As shown in Fig. 4, the heat flux between the plates is insensitive to the damping parameter across distances from 1 nm to 1000 nm. To compare this heat transfer with conventional near-field radiative heat transfer driven by a temperature difference, we use the Landauer formula for the undriven case to match the heat flux at $\eta = 0.1$ eV. The results show that the asymmetry-induced heat flux in the driven case is comparable to that of two undriven plates with an average temperature of 1650 K and a temperature difference of 10 K.

Discussion.— To observe the exponential-staircase distribution of radiative photons, both $\hbar\Omega \gg k_B T_0$ [58] and $\mu_d > k_B T_0$ should be met, ensuring visibility of the first step in $\bar{N}(\omega)$. These have been realized in various platforms for Floquet dynamics [19, 20]. The effective-distribution difference can be extracted as $\Delta\bar{N}_{\text{exp}}(\omega) = J(\omega)/T(\omega)$, where J and T are, respectively, the heat flux and transmission spectra from spectral measurements of thermal emitters [59, 60]. For near-field radiative heat transfer between two metal plates, the driving frequency should be less than the cutoff frequency of the effective transmission, i.e., $\Omega < \omega_c$. The cutoff frequency is approximated as $\omega_c = \omega_p \sqrt{a/d}$ with ω_p the plasma frequency [61] at separations of $d \gg a$. As for the asymmetry-induced heat transfer, advances in measuring near-field radiative heat transfer between planar materials [62–65] have created favorable experimental conditions for verification, and recent experiments on radiative thermal transistors [66, 67] may enable observations in temporally modulated systems. Global periodic modulation of the chemical potential can be realized by applying an AC gate voltage. Since the intriguing phenomena reported in this work are closely tied to the evanescent modes, the separation between the plates should be in the near-field region. We refer to the Supplemental Material for more details about possible setups [54].

In summary, using the nonequilibrium Green's function method, we have reported the exponential-staircase feature of photon distribution in Floquet states and the asymmetry-induced radiative heat transfer in systems with periodic modulation. The resulting heat flux is comparable to conventional near-field thermal radiation driven by a temperature difference and can be effectively tuned by the properties of plates and driving parameters. These findings provide valuable insights into the directional manipulation of radiative heat transfer through Floquet engineering.

Acknowledgments.— H.P. and J.-S.W. acknowledge support from MOE FRC tier 1 grant A-8000990-00-00. G.T. is supported by National Natural Science Foundation of China (Grant No. 12374048, and No. 12088101) and NSAF (Grant No. U2330401). The computational work for this article was fully performed on resources of the National Supercomputing Centre, Singapore (<https://www.nscc.sg>).

* panhui@nus.edu.sg

† gmtang@gscaep.ac.cn

‡ phywjs@nus.edu.sg

- [1] S. M. Rytov, *Theory of Electrical Fluctuation and Thermal Radiation* (Academy of Science of USSR, Moscow, 1953).
- [2] D. Polder and M. Van Hove, Theory of radiative heat transfer between closely spaced bodies, *Phys. Rev. B* **4**, 3303 (1971).
- [3] H. B. Callen and T. A. Welton, Irreversibility and generalized noise, *Phys. Rev.* **83**, 34 (1951).
- [4] J. B. Pendry, Radiative exchange of heat between nanostructures, *J. Phys.: Condens. Matter* **11**, 6621 (1999).
- [5] K. Joulain, J.-P. Mulet, F. Marquier, R. Carminati, and J.-J. Greffet, Surface electromagnetic waves thermally excited: Radiative heat transfer, coherence properties and Casimir forces revisited in the near field, *Surf. Sci. Rep.* **57**, 59 (2005).
- [6] A. I. Volokitin and B. N. J. Persson, Near-field radiative heat transfer and noncontact friction, *Rev. Mod. Phys.* **79**, 1291 (2007).
- [7] B. Song, A. Fiorino, E. Meyhofer, and P. Reddy, Near-field radiative thermal transport: From theory to experiment, *AIP Adv.* **5**, 053503 (2015).
- [8] X. Liu, L. Wang, and Z. M. Zhang, Near-field thermal radiation: Recent progress and outlook, *Nanoscale and Microscale Thermophys. Eng.* **19**, 98 (2015).
- [9] J. C. Cuevas and F. J. García-Vidal, Radiative heat transfer, *ACS Photonics* **5**, 3896 (2018).
- [10] S.-A. Biehs, R. Messina, P. S. Venkataram, A. W. Rodriguez, J. C. Cuevas, and P. Ben-Abdallah, Near-field radiative heat transfer in many-body systems, *Rev. Mod. Phys.* **93**, 025009 (2021).
- [11] H. Aoki, N. Tsuji, M. Eckstein, M. Kollar, T. Oka, and P. Werner, Nonequilibrium dynamical mean-field theory and its applications, *Rev. Mod. Phys.* **86**, 779 (2014).
- [12] J. E. Vázquez-Lozano and I. Liberal, Incandescent temporal metamaterials, *Nat. Commun.* **14**, 4606 (2023).
- [13] G. Tang and J.-S. Wang, Modulating near-field thermal transfer through temporal drivings: A quantum many-body theory, *Phys. Rev. B* **109**, 085428 (2024).
- [14] W. Kohn, Periodic thermodynamics, *J. Stat. Phys.* **103**, 417 (2001).
- [15] N. Tsuji, T. Oka, and H. Aoki, Correlated electron systems periodically driven out of equilibrium: Floquet+DMFT formalism, *Phys. Rev. B* **78**, 235124 (2008).
- [16] T. Kitagawa, T. Oka, A. Brataas, L. Fu, and E. Demler, Transport properties of nonequilibrium systems under the application of light: Photoinduced quantum Hall insulators without Landau levels, *Phys. Rev. B* **84**, 235108 (2011).
- [17] K. I. Seetharam, C.-E. Bardyn, N. H. Lindner, M. S. Rudner, and G. Refael, Controlled population of Floquet-Bloch states via coupling to Bose and Fermi baths, *Phys. Rev. X* **5**, 041050 (2015).
- [18] M. S. Rudner and N. H. Lindner, Band structure engineering and non-equilibrium dynamics in Floquet topological insulators, *Nat. Rev. Phys.* **2**, 229 (2020).
- [19] M. Merboldt, M. Schüler, D. Schmitt, J. P. Bange, W. Bennecke, K. Gadge, K. Pierz, H. W. Schumacher, D. Momeni, D. Steil, S. R. Manmana, M. Sentef, M. Reutz, and S. Mathias, Observation of Floquet states in graphene (2024), [arXiv:2404.12791](https://arxiv.org/abs/2404.12791).
- [20] D. Choi, M. Mogi, U. D. Giovannini, D. Azoury, B. Lv, Y. Su, H. Hübener, A. Rubio, and N. Gedik, Direct observation of Floquet-Bloch states in monolayer graphene (2024), [arXiv:2404.14392](https://arxiv.org/abs/2404.14392).
- [21] A. M. Shaltout, V. M. Shalaev, and M. L. Brongersma, Spatiotemporal light control with active metasurfaces, *Science* **364**, eaat3100 (2019).
- [22] S. Yin, E. Galiffi, and A. Alù, Floquet metamaterials, *eLight* **2**, 8 (2022).
- [23] E. Galiffi, R. Tirole, S. Yin, H. Li, S. Vezzoli, P. A. Huidobro, M. G. Silveirinha, R. Sapienza, A. Alù, and J. B. Pendry, Photonics of time-varying media, *Adv. Photonics* **4**, 014002 (2022).
- [24] S. A. R. Horsley and J. B. Pendry, Traveling wave amplification in stationary gratings, *Phys. Rev. Lett.* **133**, 156903 (2024).
- [25] Y. Sharabi, E. Lustig, and M. Segev, Disordered photonic time crystals, *Phys. Rev. Lett.* **126**, 163902 (2021).
- [26] S. Saha, O. Segal, C. Fruhling, E. Lustig, M. Segev, A. Boltasseva, and V. M. Shalaev, Photonic time crystals: a materials perspective, *Opt. Express* **31**, 8267 (2023).
- [27] E. Lustig, O. Segal, S. Saha, C. Fruhling, V. M. Shalaev, A. Boltasseva, and M. Segev, Photonic time-crystals - fundamental concepts, *Opt. Express* **31**, 9165 (2023).
- [28] H. He, S. Zhang, J. Qi, F. Bo, and H. Li, Faraday rotation in non-reciprocal photonic time-crystals, *Appl. Phys. Lett.* **122** (2023).
- [29] Z. Yu and S. Fan, Complete optical isolation created by indirect interband photonic transitions, *Nat. Photonics* **3**, 91 (2009).
- [30] Y. Hadad, J. C. Soric, and A. Alu, Breaking temporal symmetries for emission and absorption, *Proc. Natl. Acad. Sci.* **113**, 3471 (2016).
- [31] D. L. Sounas and A. Alù, Non-reciprocal photonics based on time modulation, *Nat. Photonics* **11**, 774 (2017).
- [32] P. A. Huidobro, E. Galiffi, S. Guenneau, R. V. Craster, and J. B. Pendry, Fresnel drag in space-time-modulated metamaterials, *Proc. Natl. Acad. Sci.* **116**, 24943 (2019).
- [33] E. Galiffi, P. A. Huidobro, and J. B. Pendry, Broadband non-reciprocal amplification in luminal metamaterials, *Phys. Rev. Lett.* **123**, 206101 (2019).
- [34] X. Wang, G. Ptitcyn, V. S. Asadchy, A. Díaz-Rubio, M. S. Mirmoosa, S. Fan, and S. A. Tretyakov, Nonreciprocity in bianisotropic systems with uniform time modulation, *Phys. Rev. Lett.* **125**, 266102 (2020).
- [35] Z. J. Coppens and J. G. Valentine, Spatial and temporal modulation of thermal emission, *Adv. Mater.* **29**, 1701275 (2017).
- [36] J. Kou and A. J. Minnich, Dynamic optical control of near-field

- radiative transfer, *Opt. Express* **26**, A729 (2018).
- [37] H. Li, L. J. Fernández-Alcázar, F. Ellis, B. Shapiro, and T. Kottos, Adiabatic thermal radiation pumps for thermal photonics, *Phys. Rev. Lett.* **123**, 165901 (2019).
- [38] L. J. Fernández-Alcázar, H. Li, M. Nafari, and T. Kottos, Implementation of optimal thermal radiation pumps using adiabatically modulated photonic cavities, *ACS Photonics* **8**, 2973 (2021).
- [39] M. F. Picardi, K. N. Nimje, and G. T. Papadakis, Dynamic modulation of thermal emission—A tutorial, *J. Appl. Phys.* **133**, 111101 (2023).
- [40] I. Latella, R. Messina, J. M. Rubi, and P. Ben-Abdallah, Radiative heat shuttling, *Phys. Rev. Lett.* **121**, 023903 (2018).
- [41] S. Buddhiraju, W. Li, and S. Fan, Photonic refrigeration from time-modulated thermal emission, *Phys. Rev. Lett.* **124**, 077402 (2020).
- [42] R. Yu and S. Fan, Time-modulated near-field radiative heat transfer, *Proc. Natl. Acad. Sci.* **121** (2024).
- [43] R. Yu and S. Fan, Manipulating coherence of near-field thermal radiation in time-modulated systems, *Phys. Rev. Lett.* **130**, 096902 (2023).
- [44] L. J. Fernández-Alcázar, R. Kononchuk, H. Li, and T. Kottos, Extreme nonreciprocal near-field thermal radiation via Floquet photonics, *Phys. Rev. Lett.* **126**, 204101 (2021).
- [45] S.-A. Biehs and G. S. Agarwal, Breakdown of detailed balance for thermal radiation by synthetic fields, *Phys. Rev. Lett.* **130**, 110401 (2023).
- [46] S.-A. Biehs, P. Rodriguez-Lopez, M. Antezza, and G. S. Agarwal, Nonreciprocal heat flux via synthetic fields in linear quantum systems, *Phys. Rev. A* **108**, 042201 (2023).
- [47] J.-S. Wang and J. Peng, Capacitor physics in ultra-near-field heat transfer, *Europhys. Lett.* **118**, 24001 (2017).
- [48] J.-H. Jiang and J.-S. Wang, Caroli formalism in near-field heat transfer between parallel graphene sheets, *Phys. Rev. B* **96**, 155437 (2017).
- [49] T. Zhu, Z.-Q. Zhang, Z. Gao, and J.-S. Wang, First-principles method to study near-field radiative heat transfer, *Phys. Rev. Appl.* **14**, 024080 (2020).
- [50] J. L. Wise, N. Roubinowitz, W. Belzig, and D. M. Basko, Signature of resonant modes in radiative heat current noise spectrum, *Phys. Rev. B* **106**, 165407 (2022).
- [51] A. L. Chudnovskiy, A. Levchenko, and A. Kamenev, Coulomb drag and heat transfer in strange metals, *Phys. Rev. Lett.* **131**, 096501 (2023).
- [52] J.-S. Wang, J. Peng, Z.-Q. Zhang, Y.-M. Zhang, and T. Zhu, Transport in electron-photon systems, *Front. Phys.* **18**, 43602 (2023).
- [53] J.-S. Wang and M. Antezza, Photon mediated transport of energy, linear momentum, and angular momentum in fullerene and graphene systems beyond local equilibrium, *Phys. Rev. B* **109**, 125105 (2024).
- [54] See Supplemental Material for details of derivations (photon self-energies, energy currents, and effective electron/photon distributions), proofs, and possible experimental setups, which includes Refs. [68–78].
- [55] H. Haug and A.-P. Jauho, *Quantum Kinetics in Transport and Optics of Semiconductors*, Vol. 2 (Springer, 2008).
- [56] E. M. Lifshitz and L. P. Pitaevskii, *Statistical Physics: Theory of the Condensed State*, Vol. 9 (Elsevier, 2013).
- [57] B. S. Kay, Quantum Electrostatics, Gauss’s Law, and a Product Picture for Quantum Electrodynamics; or, the Temporal Gauge Revised, *Found. Phys.* **52**, 6 (2022).
- [58] L.-k. Shi, O. Matsyshyn, J. C. W. Song, and I. S. Villadiego, Floquet Fermi liquid, *Phys. Rev. Lett.* **132**, 146402 (2024).
- [59] A. Babuty, K. Joulain, P.-O. Chapuis, J.-J. Greffet, and Y. De Wilde, Blackbody spectrum revisited in the near field, *Phys. Rev. Lett.* **110**, 146103 (2013).
- [60] S. Zare, C. P. Tripp, and S. Edalatpour, Measurement of near-field thermal emission spectra using an internal reflection element, *Phys. Rev. B* **100**, 235450 (2019).
- [61] E. H. Hwang and S. Das Sarma, Dielectric function, screening, and plasmons in two-dimensional graphene, *Phys. Rev. B* **75**, 205418 (2007).
- [62] L. Hu, A. Narayanaswamy, X. Chen, and G. Chen, Near-field thermal radiation between two closely spaced glass plates exceeding Planck’s blackbody radiation law, *Appl. Phys. Lett.* **92**, 133106 (2008).
- [63] B. Song, D. Thompson, A. Fiorino, Y. Ganjeh, P. Reddy, and E. Meyhofer, Radiative heat conductances between dielectric and metallic parallel plates with nanoscale gaps, *Nat. Nanotechnol.* **11**, 509 (2016).
- [64] S. Zhang, Y. Dang, X. Li, N. Iqbal, Y. Jin, P. K. Choudhury, M. Antezza, J. Xu, and Y. Ma, Measurement of near-field thermal radiation between multilayered metamaterials, *Phys. Rev. Appl.* **21**, 24054 (2024).
- [65] Y. Li, Y. Dang, S. Zhang, X. Li, T. Chen, P. K. Choudhury, Y. Jin, J. Xu, P. Ben-Abdallah, B.-F. Ju, and Y. Ma, Observation of heat pumping effect by radiative shuttling, *Nat. Commun.* **15**, 5465 (2024).
- [66] D. Thompson, L. Zhu, E. Meyhofer, and P. Reddy, Nanoscale radiative thermal switching via multi-body effects, *Nat. Nanotechnol.* **15**, 99 (2020).
- [67] J. W. Lim, A. Majumder, R. Mittapally, A.-R. Gutierrez, Y. Luan, E. Meyhofer, and P. Reddy, A nanoscale photonic thermal resistor for sub-second heat flow switching, *Nat. Commun.* **15**, 5584 (2024).
- [68] O. Matsyshyn, J. C. W. Song, I. S. Villadiego, and L.-k. Shi, Fermi-Dirac staircase occupation of Floquet bands and current rectification inside the optical gap of metals: An exact approach, *Phys. Rev. B* **107**, 195135 (2023).
- [69] R. Peierls, Zur Theorie des Diamagnetismus von Leitungselektronen, *Z. Phys.* **80**, 763 (1933).
- [70] M. Rodriguez-Vega, M. Vogl, and G. A. Fiete, Low-frequency and Moiré-Floquet engineering: A review, *Ann. Phys.* **435**, 168434 (2021).
- [71] J. E. Sipe, New Green-function formalism for surface optics, *J. Opt. Soc. Am. B* **4**, 481 (1987).
- [72] K. Joulain, J.-P. Mulet, F. Marquier, R. Carminati, and J.-J. Greffet, Surface electromagnetic waves thermally excited: Radiative heat transfer, coherence properties and Casimir forces revisited in the near field, *Surf. Sci. Rep.* **57**, 59 (2005).
- [73] H. H. Yap and J.-S. Wang, Radiative heat transfer as a Landauer-Büttiker problem, *Phys. Rev. E* **95**, 012126 (2017).
- [74] D. C. Langreth and P. Nordlander, Derivation of a master equation for charge-transfer processes in atom-surface collisions, *Phys. Rev. B* **43**, 2541 (1991).
- [75] H. Rostami, M. I. Katsnelson, G. Vignale, and M. Polini, Gauge invariance and Ward identities in nonlinear response theory, *Ann. Phys.* **431**, 168523 (2021).
- [76] J. H. Shirley, Solution of the Schrödinger equation with a Hamiltonian periodic in time, *Phys. Rev.* **138**, B979 (1965).
- [77] H. P. Breuer and M. Holthaus, Quantum phases and Landau-Zener transitions in oscillating fields, *Phys. Lett. A* **140**, 507 (1989).
- [78] R. Kumari, B. Seradjeh, and A. Kundu, Josephson-current signatures of unpaired Floquet Majorana bound states (2023), [arXiv:2301.07707](https://arxiv.org/abs/2301.07707).

Supplemental Material for “Asymmetry-induced radiative heat transfer in Floquet systems”

Hui Pan,^{1,*} Yuhua Ren,¹ Gaomin Tang,^{2,†} and Jian-Sheng Wang^{1,‡}

¹*Department of Physics, National University of Singapore, Singapore 117551, Republic of Singapore*

²*Graduate School of China Academy of Engineering Physics, Beijing 100193, China*

CONTENTS

A. Model and Hamiltonian	1
B. Floquet representation	2
C. Floquet electron Green’s function	3
D. Free photon Green’s function	4
E. Nonequilibrium photon Green’s function and self-energies	4
F. Derivation of the expression of photon energy currents	6
G. Effective distribution of the electrons in Floquet systems	7
H. Effective photon distribution and its asymptotic properties	8
I. Dependence of heat flux on hopping parameter difference	9
J. Possible experimental setups	9
References	10

A. Model and Hamiltonian

We investigate the radiative heat transfer between two objects due to current fluctuations. The energy transport between the two subsystems separated by a vacuum gap is mediated by an electromagnetic (EM) field. The total Hamiltonian of the open quantum system can be partitioned as [1]

$$\hat{H}_{\text{tot}} = \hat{H}_e + \hat{H}_{\text{ph}} + \hat{H}_{\text{int}}. \quad (\text{S1})$$

The electronic Hamiltonian is given by

$$\hat{H}_e = \sum_{\alpha} (\hat{H}_{\alpha} + \hat{H}_{\alpha B} + \hat{V}_{\alpha B} + \hat{V}_{\alpha B}^{\dagger}), \quad (\text{S2})$$

where $\alpha = L, R$ denotes the left and right subsystems. In the tight-binding model, the Hamiltonian of object α in second quantization is

$$\hat{H}_{\alpha} = \sum_{i,j \in \alpha} c_i^{\dagger} H_{ij} c_j, \quad (\text{S3})$$

where i and j run over all the electron sites with coordinates \mathbf{r}_i and \mathbf{r}_j of object α .

The electronic reservoir, which provides the dissipation channel for the energy current [2], is modeled with the Hamiltonian

$$\hat{H}_{\alpha B} = \sum_k \varepsilon_{k\alpha} d_{k\alpha}^{\dagger} d_{k\alpha}. \quad (\text{S4})$$

The coupling between object α and its corresponding reservoir is given by

$$\hat{V}_{\alpha B} = \sum_{k;i \in \alpha} t_{k\alpha,i} d_{k\alpha}^{\dagger} c_i. \quad (\text{S5})$$

* panhui@nus.edu.sg

† gmtang@gscaep.ac.cn

‡ phywjs@nus.edu.sg

The degrees of freedom of the reservoirs can be analytically integrated out and act as self-energies in the electron Green's functions.

The Hamiltonian of the EM field depends on the gauge chosen. In the temporal gauge [3, 4], the Hamiltonian is given in terms of the vector potential \mathbf{A} by

$$\hat{H}_{\text{ph}} = \frac{1}{2} \int dV \left[\epsilon_0 (\partial_t \mathbf{A})^2 + \mu_0^{-1} (\nabla \times \mathbf{A})^2 \right], \quad (\text{S6})$$

where ϵ_0 and μ_0 are the vacuum permittivity and permeability. The practical advantage of the temporal gauge is the reduced number of components in the physical quantities that are needed to be calculated.

The interaction between the electrons and the EM field is described by the Peierls substitution [5]. Equation (S3) is modified as

$$\hat{H}_\alpha + \hat{H}_{\text{int}} = \sum_{i,j \in \alpha} c_i^\dagger H_{ij} c_j \exp \left[\frac{e_0}{i\hbar} \int_{r_j}^{r_i} d\mathbf{r} \cdot \mathbf{A}(\mathbf{r}) \right], \quad (\text{S7})$$

where $e_0 > 0$ denotes the elementary charge. To isolate \hat{H}_{int} , we approximate the line integral with the trapezoidal rule

$$\int_{r_j}^{r_i} d\mathbf{r} \cdot \mathbf{A}(\mathbf{r}) \approx \frac{1}{2} (\mathbf{A}_i + \mathbf{A}_j) \cdot (\mathbf{r}_i - \mathbf{r}_j), \quad (\text{S8})$$

where we have used the notation $\mathbf{A}_i \equiv \mathbf{A}(\mathbf{r}_i)$. Performing a Taylor expansion to the exponential in Eq. (S7) up to second order in the lattice constant, we can write the interaction Hamiltonian as

$$\begin{aligned} \hat{H}_{\text{int}} &= \sum_{i,j,l,\mu} c_i^\dagger M_{ij}^{l\mu} c_j A_{l\mu} + \frac{1}{2} \sum_{i,j,l,l',\mu,\nu} c_i^\dagger N_{ij}^{l\mu,l'\nu} c_j A_{l\mu} A_{l'\nu} \\ &\equiv - \sum_l \mathbf{I}_l \cdot \mathbf{A}_l + \hat{H}_{\text{dia}}, \end{aligned} \quad (\text{S9})$$

where the tensor M and N are, respectively, expressed as

$$M_{ij}^{l\mu} = \frac{e_0}{2} (\delta_{il} + \delta_{jl}) V_{ij}^\mu, \quad (\text{S10})$$

$$N_{ij}^{l\mu,l'\nu} = \frac{e_0}{2i\hbar} M_{ij}^{l\mu} (r_i^\nu - r_j^\nu) (\delta_{il'} + \delta_{jl'}), \quad (\text{S11})$$

and the velocity matrix \mathbf{V} has the elements

$$V_{ij}^\mu = \frac{1}{i\hbar} H_{ij} (r_i^\mu - r_j^\mu), \quad (\text{S12})$$

which represents the velocity of the electron hopping from site j to i . Here, the indices i, j , and l denote the electron site, and $\mu = x, y, z$ labels the Cartesian directions.

B. Floquet representation

For a two-time function with the symmetry $G(t_1 + 2\pi/\Omega, t_2 + 2\pi/\Omega) = G(t_1, t_2)$, we define its Floquet representation [6–8] by

$$\begin{aligned} G(t_1, t_2) &\rightarrow \mathbf{G}(\omega) \\ G_{mn}(\omega) &\equiv \frac{\Omega}{2\pi} \int_0^{2\pi/\Omega} dt_1 \int_{-\infty}^{\infty} dt_2 G(t_1, t_2) e^{i(\omega_m t_1 - \omega_n t_2)}, \end{aligned} \quad (\text{S13})$$

where $m, n \in \mathbb{Z}$. $G_{mn}(\omega)$ can be interpreted as the (m, n) entries of an infinite block matrix $\mathbf{G}(\omega)$, and such extended Floquet matrices will be denoted in bold. Here, we have defined $\omega_m = m\Omega + \omega$. A periodic function of one argument, $H(t_1)$, can be upgraded into a two-time function by considering $H(t_1)\delta(t_1 - t_2)$, and its Floquet representation \mathbf{H} is a block Toeplitz matrix. The inverse transformation to return to the time domain is given by

$$G(t_1, t_2) = \sum_{mn} \int_{\text{BZ}} \frac{d\omega}{2\pi} G_{mn}(\omega) e^{-i(\omega_m t_1 - \omega_n t_2)}. \quad (\text{S14})$$

The integration region in Eq. (S14), the Floquet-Brillouin zone (BZ), is chosen to be $-\Omega/2 < \omega \leq \Omega/2$. Eq. (S13) allows for ω to be outside of the range given by BZ, but no new information is conveyed because of the modular property

$$G_{mn}(\omega + k\Omega) = G_{m+k, n+k}(\omega). \quad (\text{S15})$$

Nevertheless, Eq. (S15) is useful in numerical computations as the middle element (“00” block) of the Floquet matrix has the smallest truncation errors.

Below, we list several important properties of the Floquet representation that will be used later. Differentiation in the time domain becomes multiplication in Floquet representation.

$$i\hbar \frac{\partial}{\partial t_1} G(t_1, t_2) \rightarrow \mathbf{E}(\omega) \mathbf{G}(\omega), \quad (\text{S16})$$

$$i\hbar \frac{\partial}{\partial t_2} G(t_1, t_2) \rightarrow -\mathbf{G}(\omega) \mathbf{E}(\omega), \quad (\text{S17})$$

where the Floquet matrix $\mathbf{E}(\omega)$ associated with differentiation is defined as the block diagonal matrix with elements

$$E_{mn}(\omega) = \hbar(\omega + m\Omega) \delta_{mn} I. \quad (\text{S18})$$

We also have the analog of the convolution theorems [6, 9] in the Floquet representation. If A and B both have the same discrete time translational symmetry, then

$$\int dt' A(t_1, t') B(t', t_2) \rightarrow \mathbf{A}(\omega) \mathbf{B}(\omega). \quad (\text{S19})$$

and

$$\begin{aligned} C(t_1, t_2) &= A(t_1, t_2) B(t_2, t_1) \\ \rightarrow C_{mn}(\omega) &= \sum_{l_p} \int_{\text{BZ}} \frac{d\omega'}{2\pi} A_{l_p}(\omega') B_{(p-n)(l-m)}(\omega' - \omega). \end{aligned} \quad (\text{S20})$$

Eq. (S20) is useful for obtaining the polarization functions, Π , in the Floquet representation.

C. Floquet electron Green's function

The nonequilibrium electron Green's function on the Keldysh contour is defined as [10]

$$G_{ij}(\tau, \tau') = \frac{1}{i\hbar} \left\langle \mathcal{T} c_i(\tau) c_j^\dagger(\tau') \right\rangle, \quad (\text{S21})$$

where \mathcal{T} is the contour time-ordering operator and $c_i, (c_i^\dagger)$ are the annihilation (creation) operators in the Heisenberg picture. In this Supplemental Material, the time variables in Greek letters sit on the Keldysh contour while those in Latin letters are the normal ones. In the absence of coupling to the EM field, the retarded component of G satisfies the Dyson equation

$$[i\hbar\partial_t - H(t)] G^r(t, t') = \delta(t - t') I + \int dt_1 \Sigma^r(t, t_1) G^r(t_1, t'), \quad (\text{S22})$$

where $\delta(t)$ is the Dirac-delta function, and I the identity matrix. The self-energy term denoted by Σ^r describes the presence of a bath. We use the wide-band approximation, where each site is coupled to the bath independently of energy, so that the retarded self-energy in the energy domain takes the form of

$$\Sigma^r(\omega) = -i\eta \quad (\text{S23})$$

with \hbar/η having the interpretation of the electron relaxation time.

Due to Floquet's theorem, we have the discrete time-translational symmetry in G^r , which allows us to write Eq. (S22) in the Floquet representation as

$$\mathbf{G}^r(\omega) = [\mathbf{E}(\omega) + i\eta \mathbf{I} - \mathbf{H}]^{-1}, \quad (\text{S24})$$

where \mathbf{I} is the identity matrix and $\mathbf{E}(\omega)$ is previously defined in Eq. (S18). The advanced component is obtained with $G_{mn}^a(\omega) = [G_{nm}^r(\omega)]^\dagger$. The electron distribution is described by the lesser Green's function $G^<$ with

$$G_{ij}^<(t, t') = -\frac{1}{i\hbar} \langle c_j^\dagger(t') c_i(t) \rangle. \quad (\text{S25})$$

In a Floquet steady state [2, 11], the lesser Green's function can be given by the Keldysh equation as

$$G^<(t, t') = \int dt_1 \int dt_2 G^r(t, t_1) \Sigma^<(t_1 - t_2) G^a(t_2, t'). \quad (\text{S26})$$

In the Floquet representation, Eq. (S26) is written as

$$\mathbf{G}^<(\omega) = \mathbf{G}^r(\omega) \mathbf{\Sigma}^<(\omega) \mathbf{G}^a(\omega), \quad (\text{S27})$$

where $\mathbf{\Sigma}^<$ is the lesser component of the bath self-energy. We assume that the bath remains in thermal equilibrium and thus obeys the fluctuation-dissipation theorem,

$$\Sigma_{mn}^<(\omega) = -f(\omega_m) [\Sigma_{mn}^r(\omega) - \Sigma_{mn}^a(\omega)], \quad (\text{S28})$$

with

$$f(\omega) = \frac{1}{\exp[(\hbar\omega - \mu_s)/(k_B T_0)] + 1} \quad (\text{S29})$$

being the Fermi-Dirac function at temperature T_0 and chemical potential μ_s .

D. Free photon Green's function

In the temporal gauge, the Maxwell-Ampere law relates the current \mathbf{j} to the vector potential \mathbf{A} by a linear operator, v^{-1} , given by

$$-\mathbf{j} = -\epsilon_0 \frac{\partial^2}{\partial t^2} \mathbf{A} - \mu_0^{-1} \nabla \times \nabla \times \mathbf{A} \equiv v^{-1} \mathbf{A}. \quad (\text{S30})$$

For the present problem with planar geometry, the expression of $v^r(t, \mathbf{r})$, the retarded Green's function corresponding to the operator v^{-1} , can be found in the momentum and frequency domain to be [3, 12–14]

$$v^r(\omega, \mathbf{q}, z) = \frac{\mu_0}{a^2 k_0^2} \left(\frac{e^{i\gamma|z|}}{2i\gamma} \begin{bmatrix} k_0^2 - q_x^2 & -q_x q_y & -s q_x \gamma \\ -q_x q_y & k_0^2 - q_y^2 & -s q_y \gamma \\ -s q_x \gamma & -s q_y \gamma & k_0^2 - \gamma^2 \end{bmatrix} + \delta(z) \hat{z} \hat{z} \right), \quad (\text{S31})$$

where $s = \text{sgn}(z)$, a is the lattice constant, $\mathbf{q} = (q_x, q_y)$ the 2D wave vector, and $k_0 = \omega/c$. The photon propagation constant γ is defined as $\gamma = \sqrt{k_0^2 - q^2}$ for the propagating mode ($k_0 > q$), and $\gamma = i\sqrt{q^2 - k_0^2}$ for the evanescent mode ($k_0 < q$), where q is the wave vector length. In numerical calculations, we use the discrete Fourier transform instead of the continuous version. The factor of $1/a^2$ in Eq. (S31) is due to the normalization convention for space discrete Fourier transform. Since the spatial integral is replaced by a sum over all sites, the value of the 1D Dirac-delta in Eq. (S31) is represented by $1/a$.

E. Nonequilibrium photon Green's function and self-energies

The full photon Green's function is defined by the vector potential \mathbf{A} on the Keldysh contour as [1, 3]

$$D_{\mu\nu}(\mathbf{r}\tau, \mathbf{r}'\tau') = \frac{1}{i\hbar} \langle \mathcal{T} A_\mu(\mathbf{r}\tau) A_\nu(\mathbf{r}'\tau') \rangle, \quad (\text{S32})$$

with $\mu, \nu = x, y, z$ denoting the spatial directions. The retarded and lesser components of the photon Green's function are, respectively, given by

$$D_{\mu\nu}^r(\mathbf{r}t, \mathbf{r}'t') = \frac{1}{i\hbar} \theta(t - t') \langle [A_\mu(\mathbf{r}t), A_\nu(\mathbf{r}'t')] \rangle, \quad (\text{S33})$$

$$D_{\mu\nu}^<(\mathbf{r}t, \mathbf{r}'t') = \frac{1}{i\hbar} \langle A_\nu(\mathbf{r}'t') A_\mu(\mathbf{r}t) \rangle. \quad (\text{S34})$$

The vector potential are quantum operators in the Heisenberg picture, and the square brackets represent the commutator. The full Green's function D is related to the polarization Π and the free Green's function v by the Dyson equation on the Keldysh contour as

$$D(\mathbf{r}\tau, \mathbf{r}'\tau') = v(\mathbf{r}\tau, \mathbf{r}'\tau') + \sum_{ij} \int d\tau_1 \int d\tau_2 v(\mathbf{r}\tau, \mathbf{r}_i\tau_1) \Pi_{ij}(\tau_1, \tau_2) D(\mathbf{r}_j\tau_2, \mathbf{r}'\tau'). \quad (\text{S35})$$

From Langreth's theorem [15], the retarded component of D satisfies the Dyson equation, written in Floquet representation as

$$\mathbf{D}^r = \mathbf{v} + \mathbf{v}\mathbf{\Pi}^r \mathbf{D}^r. \quad (\text{S36})$$

The lesser photon Green's function describes the photon distribution and is again related to the retarded one by the Keldysh equation

$$\mathbf{D}^< = \mathbf{D}^r (\mathbf{\Pi}^< + \mathbf{\Pi}_\infty^<) \mathbf{D}^a. \quad (\text{S37})$$

The extra term $\mathbf{\Pi}_\infty^<$ called the bath at infinity represents energy dissipation into the vacuum. It can be formally written as

$$\mathbf{\Pi}_\infty^r = \frac{1}{2} [-v^{-1} + (v^{-1})^\dagger]. \quad (\text{S38})$$

In frequency and momentum domain, $\mathbf{\Pi}_\infty^a = (\mathbf{\Pi}_\infty^r)^\dagger$ and $\mathbf{\Pi}_\infty^<$ is determined by the fluctuation-dissipation theorem at zero temperature.

Based on the interaction Hamiltonian [Eq. (S9)], the total polarization $\mathbf{\Pi}$ is a sum of a paramagnetic term $\mathbf{\Pi}^{\text{RPA}}$ and a diamagnetic term $\mathbf{\Pi}^{\text{dia}}$,

$$\Pi_{l\mu, l'\nu}(\tau, \tau') = \Pi_{l\mu, l'\nu}^{\text{RPA}}(\tau, \tau') + \Pi_{l\mu, l'\nu}^{\text{dia}}(\tau, \tau'). \quad (\text{S39})$$

The paramagnetic term $\mathbf{\Pi}^{\text{RPA}}$ under the random phase approximation (RPA) is

$$\Pi_{l\mu, l'\nu}^{\text{RPA}}(\tau, \tau') = \frac{1}{i\hbar} \langle \mathcal{T} I_{l\mu}(\tau) I_{l'\nu}(\tau') \rangle, \quad (\text{S40})$$

and $\mathbf{\Pi}^{\text{dia}}$ is given later [Eq. (S45)] in momentum space. The retarded photon self-energy $\mathbf{\Pi}^r$ can be interpreted as a linear response of the induced current in matter, $\mathbf{j}^{\text{ind}} = -\mathbf{\Pi}^r \mathbf{A}$. The photon self-energy $\mathbf{\Pi}$ is obtained through a diagrammatic expansion, with the interaction from the Peierls substitution Hamiltonian, Eq. (S9), taking the contributions linear in \mathbf{A} with the RPA and quadratic in \mathbf{A} for the diamagnetic term. The expressions of the self-energies under the RPA can be obtained from two electron Green's functions with

$$\Pi_{l\mu, l'\nu}^{\text{RPA}}(\tau, \tau') = -2i\hbar \sum_{ijkp} M_{ij}^{l\mu} G_{jk}(\tau, \tau') M_{kp}^{l'\nu} G_{pi}(\tau', \tau). \quad (\text{S41})$$

where $M_{pq}^{i\mu}$ is the local current operator between site p and site q as defined in Eq. (S10). The additional factor of 2 accounts for the spin degeneracy of the electrons. Its components are obtained using Langreth's theorem as

$$\Pi_{l\mu, l'\nu}^{\text{RPA}, <} (t, t') = -2i\hbar \text{tr} [M^{l\mu} G^<(t, t') M^{l'\nu} G^>(t', t)], \quad (\text{S42a})$$

$$\Pi_{l\mu, l'\nu}^{\text{RPA}, >} (t, t') = -2i\hbar \text{tr} [M^{l\mu} G^>(t, t') M^{l'\nu} G^<(t', t)], \quad (\text{S42b})$$

$$\Pi_{l\mu, l'\nu}^{\text{RPA}, r} (t, t') = -2i\hbar \text{tr} [M^{l\mu} G^r(t, t') M^{l'\nu} G^<(t', t) + M^{l\mu} G^<(t, t') M^{l'\nu} G^a(t', t)], \quad (\text{S42c})$$

$$\Pi_{l\mu, l'\nu}^{\text{RPA}, a} (t, t') = -2i\hbar \text{tr} [M^{l\mu} G^a(t, t') M^{l'\nu} G^<(t', t) + M^{l\mu} G^<(t, t') M^{l'\nu} G^r(t', t)]. \quad (\text{S42d})$$

One benefit of the trace notation [Eqs. (S42a)-(S42d)] instead of summing over indices [Eq. (S41)] is the freedom in the choice of basis states. For systems with translational invariance, working in the momentum basis is usually preferred. In momentum space, Eq. (S10) is

$$\begin{aligned} M_{\mathbf{k}\mathbf{k}'}^{q\mu} &= \frac{1}{N^{3/2}} \sum_{mnl} e^{i(-\mathbf{k}\cdot\mathbf{r}_m + \mathbf{k}'\cdot\mathbf{r}_n - \mathbf{q}\cdot\mathbf{r}_l)} M_{mn}^{l\mu} \\ &= \frac{e_0}{\sqrt{N}} \frac{V^\mu(\mathbf{k}) + V^\mu(\mathbf{k}')}{2} \delta_{\mathbf{q}, \mathbf{k}' - \mathbf{k}}, \end{aligned} \quad (\text{S43})$$

with N being the total number of lattice sites, and the expression for $V^\mu(\mathbf{k})$ is given later in Eq. (S64). The polarization functions are also diagonal in the momentum basis, in the sense that they only require one \mathbf{q} index instead of two. Taking the lesser component as an example, we have

$$\begin{aligned}\Pi_{\mu\nu}^{\text{RPA},<}(\mathbf{q}, t, t') &= \frac{1}{N} \sum_{l,l'} e^{-i\mathbf{q}\cdot(\mathbf{r}_l - \mathbf{r}_{l'})} \Pi_{\mu\nu}^<(\mathbf{r}_l t, \mathbf{r}_{l'} t') \\ &= -2i\hbar \sum_{\mathbf{k}} M_{\mathbf{k}-\mathbf{q},\mathbf{k}}^{q\mu} G_{\mathbf{k}}^<(t, t') M_{\mathbf{k},\mathbf{k}-\mathbf{q}}^{-q\nu} G_{\mathbf{k}-\mathbf{q}}^>(t', t).\end{aligned}\quad (\text{S44})$$

The retarded component Π^r has a contribution due to the diamagnetic part of the current [16]. In the long wavelength limit, the diamagnetic part of Π can be determined by gauge invariance [17] to be

$$\Pi_{\mu\nu}^{\text{dia}}(\mathbf{q}, t, t') = -\delta(t - t') \frac{\Omega}{2\pi} \int_0^{2\pi/\Omega} dt_1 \int_{-\infty}^{\infty} dt_2 \Pi_{\mu\nu}^{\text{RPA}}(\mathbf{0}, t_1, t_2). \quad (\text{S45})$$

As a function of the electron Green's function G , Π is diagonal in subsystem space with

$$\Pi = \begin{bmatrix} \Pi_L & 0 \\ 0 & \Pi_R \end{bmatrix} \quad (\text{S46})$$

Since Π is only non-zero on the lattice sites, the relevant coordinates of D in calculating energy current are those of the electrons, as shown in Eq. (S51). Therefore, it is convenient to partition v and D in numerical calculation using subsystem space as shown below with

$$v = \begin{bmatrix} v_{LL} & v_{LR} \\ v_{RL} & v_{RR} \end{bmatrix}, \quad D = \begin{bmatrix} D_{LL} & D_{LR} \\ D_{RL} & D_{RR} \end{bmatrix}. \quad (\text{S47})$$

To obtain the Floquet representation of the polarization function, we utilize the Floquet convolution theorem [Eq. (S20)]. E.g., Eq. (S44) can be rewritten as

$$[\Pi_{\mu\nu}^{\text{RPA},<}(\mathbf{q}, \omega)]_{mn} = -2i\hbar \sum_{\mathbf{k}} \int_{\text{BZ}} \frac{d\omega'}{2\pi} \sum_{lp} M_{\mathbf{k}-\mathbf{q},\mathbf{k}}^{q\mu} [\mathbf{G}_{\mathbf{k}}^<(\omega')]_{lp} M_{\mathbf{k},\mathbf{k}-\mathbf{q}}^{-q\nu} [\mathbf{G}_{\mathbf{k}-\mathbf{q}}^>(\omega' - \omega)]_{(p-n)(l-m)}. \quad (\text{S48})$$

F. Derivation of the expression of photon energy currents

Here, we derive the energy current from the perspective of the EM field. We start from Poynting's theorem

$$-\partial_t u = \nabla \cdot \mathbf{S} + \mathbf{j} \cdot \mathbf{E}, \quad (\text{S49})$$

where \mathbf{S} is the Poynting vector and $u = (\epsilon_0 E^2 + B^2/\mu_0)/2$ is the energy density. By integrating over the volume around object α and using Gauss's theorem, Eq. (S49) can be rewritten as

$$I_\alpha(t) \equiv \oint_\alpha \langle \mathbf{S} \rangle \cdot d\boldsymbol{\Sigma} = - \int_\alpha d\mathbf{r} \langle \mathbf{j} \cdot \mathbf{E} \rangle - \int_\alpha d\mathbf{r} \langle \partial_t u \rangle, \quad (\text{S50})$$

The ensemble average is defined as $\langle \dots \rangle = \text{tr}(\hat{\rho} \dots)$, where $\hat{\rho}$ is the density-matrix operator. The right-hand side consists of two terms: the first term describes Joule heating by the electric current, while the second term describes the energy change rate of the field.

In steady state, the time average of the second term vanishes, and thus the average energy current flowing out of an object is solely due to Joule heating. The energy current can be expressed in terms of the photon Green's function as

$$\begin{aligned}I_\alpha(t) &= - \int_\alpha d\mathbf{r} \left[\frac{\partial}{\partial t'} \sum_{\mu,\nu} v_{\mu\nu}^{-1}(\mathbf{r}t, \mathbf{r}t) \langle A_\nu(\mathbf{r}t) A_\mu(\mathbf{r}t') \rangle \right] \Big|_{t'=t} \\ &= - \frac{i\hbar}{2} \int_\alpha d\mathbf{r} \left\{ \frac{\partial}{\partial t'} \text{tr} [v^{-1}(\mathbf{r}t, \mathbf{r}t) D^K(\mathbf{r}t, \mathbf{r}t')] \right\} \Big|_{t'=t}.\end{aligned}\quad (\text{S51})$$

where the trace is taken over the directions μ . The reason for using the Keldysh Green's function D^K is that the physical observable of the energy current must be real. The product of two arbitrary Hermitian operators need not be Hermitian, whereas

the symmetrized version does ensure a Hermitian result. Using the Keldysh equation and the Dyson equation, the energy current can be further expressed in terms of the self-energies Π and the Green's functions D as

$$I_\alpha(t) = -\frac{i\hbar}{2} \int_\alpha d\mathbf{r} \int dt_1 \frac{\partial}{\partial t'} \text{tr} \left[\Pi_\alpha^r(\mathbf{r}t, \mathbf{r}t_1) D^K(\mathbf{r}t_1, \mathbf{r}t') + \Pi_\alpha^K(\mathbf{r}t, \mathbf{r}t_1) D^a(\mathbf{r}t_1, \mathbf{r}t') \right] \Big|_{t'=t}. \quad (\text{S52})$$

The above expression is valid for arbitrary time dependence. For the special case of periodic drive, the energy current averaged over one period is a meaningful quantity. We can calculate the average current using the Floquet representation (Sec. B) with

$$\bar{I}_\alpha = \int_{\text{BZ}} \frac{d\omega}{4\pi} \text{Tr} \left[\mathbf{E} (\mathbf{\Pi}_\alpha^r \mathbf{D}^K + \mathbf{D}_\alpha^K \mathbf{\Pi}_\alpha^a) \right]. \quad (\text{S53})$$

where the symbol ‘‘Tr’’ denotes tracing over the directions μ , the electron sites and the Floquet indices. Eq. (S53) is a generalization of the Meir-Wingreen formula [16] for the energy transport in Floquet space under periodic modulation. Using the symmetries of the Floquet representation, one can alternatively express the energy current as

$$\bar{I}_\alpha = - \int_{\text{BZ}} \frac{d\omega}{4\pi} \text{Tr} \left[\mathbf{E} (\mathbf{D}^r \mathbf{\Pi}_\alpha^K + \mathbf{D}^K \mathbf{\Pi}_\alpha^a) \right]. \quad (\text{S54})$$

An alternative approach from the perspective of electron transport is shown in Ref. [9], in which a similar expression in form as Eq. (S53) is also given by considering the Coulomb interaction.

G. Effective distribution of the electrons in Floquet systems

The solutions of the Schrödinger equation with a time-periodic Hamiltonian are linear combinations of the Floquet states [6, 8, 11, 18, 19]

$$|\Psi_a(t)\rangle = e^{-i\varepsilon_a t/\hbar} |u_a(t)\rangle, \quad (\text{S55})$$

where ε_a is the quasienergy defined up to integer multiples of $\hbar\Omega$. Floquet theorem states that $|u_a(t)\rangle = |u_a(t + 2\pi/\Omega)\rangle$ has the same periodicity as $H(t)$, and thus admits a Fourier series expansion,

$$|u_a(t)\rangle = \sum_n e^{-in\Omega t} |u_a^n\rangle. \quad (\text{S56})$$

The Floquet states are normalized with $\sum_n \langle u_a^n | u_b^n \rangle = \delta_{ab}$. By analyzing the Fourier components of the Schrödinger equation, we get the following eigenvalue equation in Floquet representation,

$$(\varepsilon_a - p\hbar\Omega) |\mathbf{u}_a^p\rangle = (\mathbf{H} - \hbar\Omega) |\mathbf{u}_a^p\rangle, \quad (\text{S57})$$

where $|\mathbf{u}_a^p\rangle$ is a vertically-stacked column vector in Floquet space with the entry in the n th block-row being $(|\mathbf{u}_a^p\rangle)_n = |u_a^{n-p}\rangle$. Notice that if $|\mathbf{u}_a^0\rangle$ is an eigenvector with eigenvalue ε_a , then $|\mathbf{u}_a^p\rangle$ is an eigenvector with eigenvalue $(\varepsilon_a - p\hbar\Omega)$. The index p keeps track of such harmonics arising from the same Floquet state, which we consider to have the same a . Assuming that the eigenvectors are complete, Eq. (S24) admits the following spectral decomposition

$$\mathbf{G}^r(\omega) = \sum_{a,p} \frac{|\mathbf{u}_a^p\rangle \langle \mathbf{u}_a^p|}{\hbar(\omega + p\Omega) + i\eta - \varepsilon_a}. \quad (\text{S58})$$

$\mathbf{G}^a(\omega)$ is expanded in the same way with the final expression differing by a minus sign in front of η . We can compute $\mathbf{G}^<(\omega)$ using Eq. (S27), and their elements are

$$G_{mn}^<(\omega) = 2i\eta \sum_{\substack{l,a,b, \\ p,q}} \frac{|u_a^{m-p}\rangle \langle u_a^{l-p}|}{\hbar(\omega + p\Omega) + i\eta - \varepsilon_a} f(\omega_l) \frac{|u_b^{l-q}\rangle \langle u_b^{n-q}|}{\hbar(\omega + q\Omega) - i\eta - \varepsilon_b}. \quad (\text{S59})$$

The lesser Green's function encodes information about the electron steady-state distribution under a periodic drive. In the case of a weak coupling to the bath $\eta \rightarrow 0^+$, Eq. (S59) can be greatly simplified by

$$\begin{aligned} G_{mn}^<(\omega) &= 2\pi i \sum_{a,p} |u_a^{m-p}\rangle \langle u_a^{n-p}| \delta(\hbar\omega_p - \varepsilon_a) \sum_l \langle u_a^{l-p} | u_a^{l-p} \rangle f(\omega_l) \\ &= 2\pi i \sum_{a,p} |u_a^{m-p}\rangle \langle u_a^{n-p}| \delta(\hbar\omega_p - \varepsilon_a) \bar{f}_a, \end{aligned} \quad (\text{S60})$$

with the effective electron distribution \bar{f} as [2, 20, 21]

$$\bar{f}_a \equiv \sum_l \langle u_a^l | u_a^l \rangle f(\varepsilon_a/\hbar + l\Omega). \quad (\text{S61})$$

The effective electron distribution accounts for all the energy levels differing by multiples of $\hbar\Omega$ from the ε_a Floquet state. The greater electron Green's function $G^>$ can be treated in the same way with

$$G_{mn}^>(\omega) = 2\pi i \sum_{a,p} |u_a^{m-p}\rangle \langle u_a^{n-p}| \delta(\hbar\omega_p - \varepsilon_a) (\bar{f}_a - 1). \quad (\text{S62})$$

H. Effective photon distribution and its asymptotic properties

We now derive the analytical formula of the effective photon distribution for a metal plate under driving in the $\eta \rightarrow 0^+$ limit. For the square-lattice model, the tight-binding electron Hamiltonian with a periodic potential modulation is diagonal in momentum space with the dispersion given by

$$H(\mathbf{k}, t) = \varepsilon_{\mathbf{k}} + \mu(t) = -2t_0 [\cos(k_x a) + \cos(k_y a)] + 2\mu_d \cos(\Omega t) \quad (\text{S63})$$

where a is the lattice constant, t_0 means the nearest-neighbor hopping parameter, and the components of wave vector $k_x, k_y \in (-\pi/a, \pi/a]$. We consider the case where the system is periodically modulated by a time-varying potential $2\mu_d \cos(\Omega t)$. The velocity operator \mathbf{V} in Eq. (S41) is also diagonal in momentum space with the elements given by

$$v^\mu(\mathbf{k}) = \frac{2at}{\hbar} \sin(k_\mu a). \quad (\text{S64})$$

With the velocity matrix, the local current density operator needed to compute Π [Eqs. (S42a)-(S42d)] can be defined using Eq. (S10).

Our driving potential is chosen in a way that the Hamiltonian commutes with itself at all times. In the Floquet representation, we mentioned that G^r can be obtained by numerical diagonalization, but it can also be expanded exactly using the Jacobi-Anger expansion. Under a uniform drive, the weights in Eq. (S61) do not depend on the Floquet index and are given by

$$\langle u_a^l | u_a^l \rangle = [J_l(\kappa)]^2, \quad (\text{S65})$$

where $\kappa = 2\mu_d/(\hbar\Omega)$ and J_l is the l th order Bessel function of the first kind. As such, we can rewrite Eq. (S60) in time domain and momentum space as

$$G_{\mathbf{k}}^<(t, t') = \frac{-\bar{f}_{\mathbf{k}}}{i\hbar} \Psi_{\mathbf{k}}(t) \Psi_{\mathbf{k}}(t')^*, \quad (\text{S66})$$

where

$$\Psi_{\mathbf{k}}(t) = \exp(-i\varepsilon_{\mathbf{k}} t/\hbar) \exp[-i\kappa \cos(\Omega t)] \quad (\text{S67})$$

is a complex number that describes the phase of the quantum state labeled by \mathbf{k} .

Having computed the electron Green's functions, the polarization can be obtained using Eq. (S44), and the results are

$$\Pi_{\mu\nu}^{\text{RPA},<}(\mathbf{q}, t, t') = \frac{2}{i\hbar} \frac{e^2}{N} \sum_{\mathbf{k}} \exp\left[\frac{(\varepsilon_{\mathbf{k}} - \varepsilon_{\mathbf{k}-\mathbf{q}})(t-t')}{i\hbar}\right] \bar{f}_{\mathbf{k}}(1 - \bar{f}_{\mathbf{k}-\mathbf{q}}) \frac{v_{\mathbf{k}}^\mu + v_{\mathbf{k}-\mathbf{q}}^\mu}{2} \frac{v_{\mathbf{k}}^\nu + v_{\mathbf{k}-\mathbf{q}}^\nu}{2}, \quad (\text{S68a})$$

$$\Pi_{\mu\nu}^{\text{RPA},>}(\mathbf{q}, t, t') = \frac{2}{i\hbar} \frac{e^2}{N} \sum_{\mathbf{k}} \exp\left[\frac{(\varepsilon_{\mathbf{k}} - \varepsilon_{\mathbf{k}-\mathbf{q}})(t-t')}{i\hbar}\right] \bar{f}_{\mathbf{k}-\mathbf{q}}(1 - \bar{f}_{\mathbf{k}}) \frac{v_{\mathbf{k}}^\mu + v_{\mathbf{k}-\mathbf{q}}^\mu}{2} \frac{v_{\mathbf{k}}^\nu + v_{\mathbf{k}-\mathbf{q}}^\nu}{2}. \quad (\text{S68b})$$

The summation should be replaced with an integral in the limit where $N \rightarrow \infty$. When compared to the equilibrium version, the only difference is that the equilibrium distribution $f(\varepsilon_{\mathbf{k}}/\hbar)$ has been replaced with the effective distribution $\bar{f}_{\mathbf{k}}$. Since all the Π above are functions of $t - t'$, the Floquet representation is unnecessary here and we can do the usual Fourier transform in $t - t'$.

It is also useful to define the spectral function as

$$\mathcal{A}_{\mu\nu}(\mathbf{q}, \omega) \equiv \text{Im} [\Pi_{\mu\nu}^{\text{RPA},r}(\mathbf{q}, \omega) - \Pi_{\mu\nu}^{\text{RPA},a}(\mathbf{q}, \omega)] = 2 \text{Im} [\Pi_{\mu\nu}^{\text{RPA},r}(\mathbf{q}, \omega)]. \quad (\text{S69})$$

For the equilibrium case, we have the fluctuation-dissipation theorem

$$\Pi_{\mu\nu}^{\text{RPA},<}(\mathbf{q}, \omega) = i\mathcal{A}_{\mu\nu}(\mathbf{q}, \omega)N(\omega, T), \quad (\text{S70a})$$

$$\Pi_{\mu\nu}^{\text{RPA},>}(\mathbf{q}, \omega) = i\mathcal{A}_{\mu\nu}(\mathbf{q}, \omega)[N(\omega, T) + 1] \quad (\text{S70b})$$

with $N(\omega, T) = 1/[\exp(\hbar\omega/k_B T) - 1]$ the Bose-Einstein distribution. For the nonequilibrium case with drivings, the *effective* distribution of the photon occupation can be defined as

$$\bar{N}(\mathbf{q}, \omega) = \frac{\text{Tr}[\text{Im}\mathbf{\Pi}^<(\mathbf{q}, \omega)]}{\text{Tr}[\mathcal{A}(\mathbf{q}, \omega)]}, \quad (\text{S71})$$

which we find can be further expressed analytically in terms of a weighted sum of the effective electron distribution \bar{f} as

$$\bar{N}(\mathbf{q}, \omega) = \frac{\sum_{\mathbf{k}} W_{\mathbf{k},\mathbf{q}}(\omega) \bar{f}(\varepsilon_{\mathbf{k}}) [1 - \bar{f}(\varepsilon_{\mathbf{k}} - \hbar\omega)]}{\sum_{\mathbf{k}} W_{\mathbf{k},\mathbf{q}}(\omega) [\bar{f}(\varepsilon_{\mathbf{k}} - \hbar\omega) - \bar{f}(\varepsilon_{\mathbf{k}})]} \quad (\text{S72})$$

with $W_{\mathbf{k},\mathbf{q}}(\omega) \equiv |\mathbf{v}_{\mathbf{k}} + \mathbf{v}_{\mathbf{k}-\mathbf{q}}|^2 \delta(\varepsilon_{\mathbf{k}} - \varepsilon_{\mathbf{k}-\mathbf{q}} - \hbar\omega)$ the weight function.

Now, we show the asymptotic behavior $\bar{N} \propto \mu_d^2$ for $\kappa = 2\mu_d/\hbar\Omega \ll 1$, using a two-level model. For the simple model with the site distance of a , the hopping parameter of t_0 , and the two energies of ε and ε' ($\varepsilon > \varepsilon'$), Eq. (S72) can be simplified to $\bar{N} = \bar{f}(\varepsilon) [1 - \bar{f}(\varepsilon')] / [\bar{f}(\varepsilon') - \bar{f}(\varepsilon)]$ by canceling the weighted function W , as the \mathbf{k} -dependent electron velocity $\mathbf{v}_{\mathbf{k}}$ is replaced by constant at_0/\hbar . We try to find the lowest-order dependence of \bar{N} on κ , since we have assumed $\kappa \ll 1$. Figure S1(a) shows a typical pattern of the two-energy levels, where ε and ε' are located at the two sides of the Fermi energy, respectively. We note that $\bar{f} \sim \kappa^2$ when $\kappa \ll 1$, which gives the jump of the first step. In this case, we obtain $\bar{N} \propto \kappa^4$, which does not have the lowest-order dependence on κ . Figure S1(b) and S1(c) show another two possible patterns where one of the energy levels is located at the Fermi surface because of the broadening of the Fermi level at finite temperatures. In these two cases, we obtain $\bar{N} \propto \kappa^2$ and consequently $\bar{N} \propto \mu_d^2$.

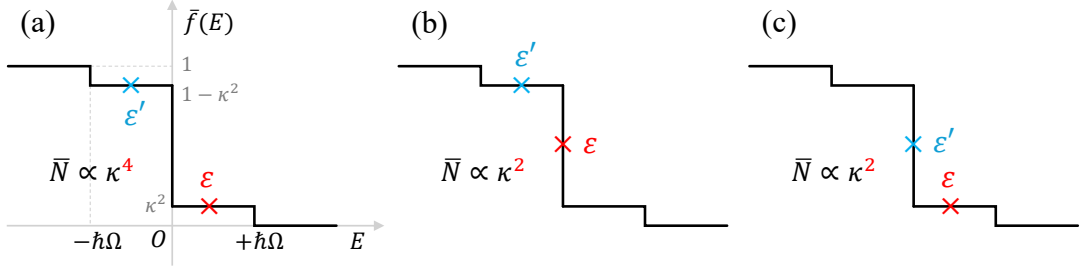


FIG. S1. Illustrations of typical patterns of electron occupation in a two-level system and the corresponding asymptotics of \bar{N} respect to $\kappa \equiv 2\mu_d/\hbar\Omega$ for $\kappa \ll 1$. (a) shows a typical pattern, which gives the asymptotics $\bar{N} \propto \kappa^4$; (b) and (c) contribute the lowest-order also most important asymptotics $\bar{N} \propto \kappa^2$, sharing same axes with (a).

I. Dependence of heat flux on hopping parameter difference

As shown in Fig. S2(a), the heat flux increases with the hopping parameter difference $t_L - t_R$ first. As the difference increases further, the heat flux begins to decrease when $t_R = 0.1$ eV. Figures S2(b) and S2(c) show the heat-flux maps when $t_R = 0.8$ eV and 0.1 eV, respectively. In contrast to Fig. S2(b), the transmission region of evanescent mode ($c|\mathbf{q}| > \omega$) in Fig. S2(c) splits into two plasmon dispersion regions, which is due to the large mismatch of plasmon frequency between the two plates.

J. Possible experimental setups

Following the discussion about the possibility of experimental realizations in the main text, here we provide two possible experimental setups, as illustrated in Fig. S3(a) and S3(b), with face-to-face and side-by-side geometries. The distance d between two material layers in Fig. S3(a) can be controlled by the thickness of the photoresist layers. A periodic chemical potential driving is realized by applying an out-of-plane AC electric field via a gate voltage with the amplitude $V_g = 2\mu_d/e_0$. As the barrier and the heat bath of electrons, the gate-oxide layer should be in contact with heaters and temperature sensors to maintain the identical

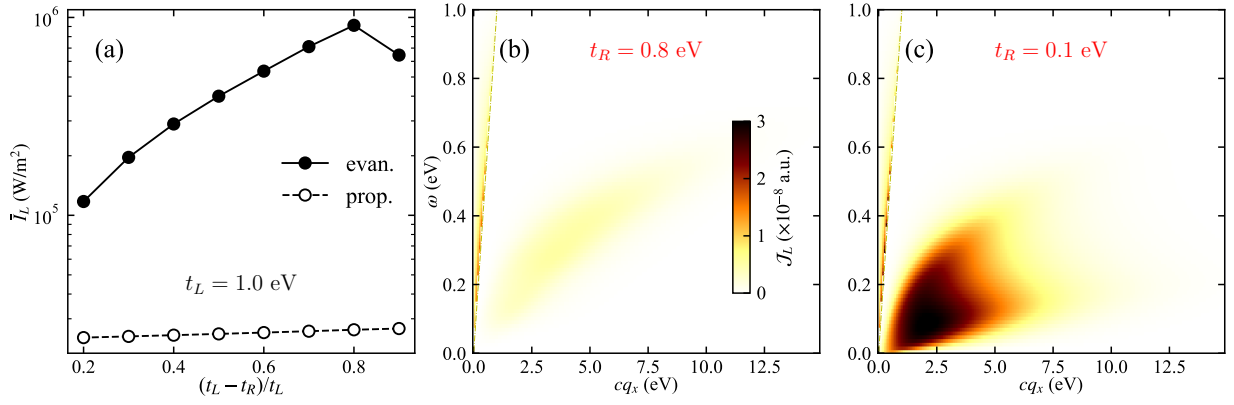


FIG. S2. (a) The heat flux changes with the relative hopping difference $(t_L - t_R)/t_L$ with $t_R = 1.0$ eV. The heat flux maps of the left plate with (b) $t_R = 0.8$ eV and (c) $t_R = 0.1$ eV. (b) and (c) share the same color bar.

bath temperatures both sides. The observation of the asymmetry-induced heat transfer requires to exclude the influence of other factors such as the Joule heating from the equivalent series resistance of capacitors and the heat conduction across other contacts (e.g., the gate oxide and photoresist layers). Given the advances in the experimental measurements of the near-field heat transfer in mesoscopic to macroscopic planar systems [22–27], we believe such setups can be realized in experiments.

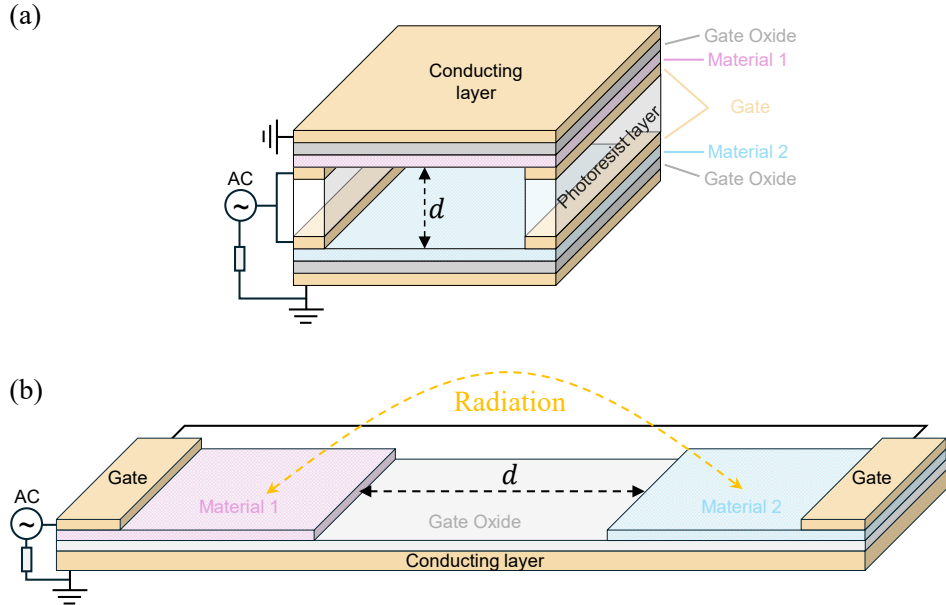


FIG. S3. Illustrations of possible experimental setups with (a) face-to-face and (b) side-by-side geometries.

-
- [1] J.-S. Wang, J. Peng, Z.-Q. Zhang, Y.-M. Zhang, and T. Zhu, Transport in electron-photon systems, *Front. Phys.* **18**, 43602 (2023).
 [2] O. Matsyshyn, J. C. W. Song, I. S. Villadiego, and L.-k. Shi, Fermi-Dirac staircase occupation of Floquet bands and current rectification inside the optical gap of metals: An exact approach, *Phys. Rev. B* **107**, 195135 (2023).
 [3] E. M. Lifshitz and L. P. Pitaevskii, *Statistical Physics: Theory of the Condensed State*, Vol. 9 (Elsevier, 2013).
 [4] B. S. Kay, Quantum Electrostatics, Gauss's Law, and a Product Picture for Quantum Electrodynamics; or, the Temporal Gauge Revised, *Found. Phys.* **52**, 6 (2022).
 [5] R. Peierls, Zur Theorie des Diamagnetismus von Leitungselektronen, *Z. Phys.* **80**, 763 (1933).
 [6] N. Tsuji, T. Oka, and H. Aoki, Correlated electron systems periodically driven out of equilibrium: Floquet + DMFT formalism, *Phys. Rev. B* **78**, 235124 (2008).

- [7] H. Aoki, N. Tsuji, M. Eckstein, M. Kollar, T. Oka, and P. Werner, Nonequilibrium dynamical mean-field theory and its applications, *Rev. Mod. Phys.* **86**, 779 (2014).
- [8] M. Rodriguez-Vega, M. Vogl, and G. A. Fiete, Low-frequency and Moiré–Floquet engineering: A review, *Ann. Phys.* **435**, 168434 (2021).
- [9] G. Tang and J.-S. Wang, Modulating near-field thermal transfer through temporal drivings: A quantum many-body theory, *Phys. Rev. B* **109**, 085428 (2024).
- [10] H. Haug and A.-P. Jauho, *Quantum Kinetics in Transport and Optics of Semiconductors*, Vol. 2 (Springer, 2008).
- [11] W. Kohn, Periodic thermodynamics, *J. Stat. Phys.* **103**, 417 (2001).
- [12] J. E. Sipe, New Green-function formalism for surface optics, *J. Opt. Soc. Am. B* **4**, 481 (1987).
- [13] K. Joulain, J.-P. Mulet, F. Marquier, R. Carminati, and J.-J. Greffet, Surface electromagnetic waves thermally excited: Radiative heat transfer, coherence properties and Casimir forces revisited in the near field, *Surf. Sci. Rep.* **57**, 59 (2005).
- [14] H. H. Yap and J.-S. Wang, Radiative heat transfer as a Landauer–Büttiker problem, *Phys. Rev. E* **95**, 012126 (2017).
- [15] D. C. Langreth and P. Nordlander, Derivation of a master equation for charge-transfer processes in atom-surface collisions, *Phys. Rev. B* **43**, 2541 (1991).
- [16] J.-S. Wang and M. Antezza, Photon mediated transport of energy, linear momentum, and angular momentum in fullerene and graphene systems beyond local equilibrium, *Phys. Rev. B* **109**, 125105 (2024).
- [17] H. Rostami, M. I. Katsnelson, G. Vignale, and M. Polini, Gauge invariance and Ward identities in nonlinear response theory, *Ann. Phys.* **431**, 168523 (2021).
- [18] J. H. Shirley, Solution of the Schrödinger equation with a Hamiltonian periodic in time, *Phys. Rev.* **138**, B979 (1965).
- [19] H. P. Breuer and M. Holthaus, Quantum phases and Landau-Zener transitions in oscillating fields, *Phys. Lett. A* **140**, 507 (1989).
- [20] K. I. Seetharam, C.-E. Bardyn, N. H. Lindner, M. S. Rudner, and G. Refael, Controlled population of Floquet-Bloch states via coupling to Bose and Fermi baths, *Phys. Rev. X* **5**, 041050 (2015).
- [21] R. Kumari, B. Seradjeh, and A. Kundu, Josephson-current signatures of unpaired Floquet Majorana bound states (2023), [arXiv:2301.07707](https://arxiv.org/abs/2301.07707).
- [22] L. Hu, A. Narayanaswamy, X. Chen, and G. Chen, Near-field thermal radiation between two closely spaced glass plates exceeding Planck’s blackbody radiation law, *Appl. Phys. Lett.* **92**, 133106 (2008).
- [23] B. Song, D. Thompson, A. Fiorino, Y. Ganjeh, P. Reddy, and E. Meyhofer, Radiative heat conductances between dielectric and metallic parallel plates with nanoscale gaps, *Nat. Nanotechnol.* **11**, 509 (2016).
- [24] S. Zhang, Y. Dang, X. Li, N. Iqbal, Y. Jin, P. K. Choudhury, M. Antezza, J. Xu, and Y. Ma, Measurement of near-field thermal radiation between multilayered metamaterials, *Phys. Rev. Appl.* **21**, 24054 (2024).
- [25] Y. Li, Y. Dang, S. Zhang, X. Li, T. Chen, P. K. Choudhury, Y. Jin, J. Xu, P. Ben-Abdallah, B.-F. Ju, and Y. Ma, Observation of heat pumping effect by radiative shuttling, *Nat. Commun.* **15**, 5465 (2024).
- [26] D. Thompson, L. Zhu, E. Meyhofer, and P. Reddy, Nanoscale radiative thermal switching via multi-body effects, *Nat. Nanotechnol.* **15**, 99 (2020).
- [27] J. W. Lim, A. Majumder, R. Mittapally, A.-R. Gutierrez, Y. Luan, E. Meyhofer, and P. Reddy, A nanoscale photonic thermal transistor for sub-second heat flow switching, *Nat. Commun.* **15**, 5584 (2024).